Towards milli-Hertz laser frequency noise on a chip

Heming Wang[1,*], Lue Wu[1,*], Zhiquan Yuan[1,*], and Kerry Vahala[1,†]
[1]T. J. Watson Laboratory of Applied Physics, California Institute of Technology, Pasadena, CA, USA
[*]These authors contributed equally.
[†]Corresponding author: vahala@caltech.edu

Narrow-linewidth lasers are important to many applications spanning precision metrology to sensing systems. Their miniaturization in the form of on-chip lasers is receiving increasing attention. Here, a noise level that is consistent with a fundamental frequency noise of 9 mHz·Hz/Hz linewidth (60 mHz linewidth) is measured in a Brillouin laser. The results leverage ultra-high-Q silica-on-silicon resonators and point towards a new performance target for chip-based laser platforms.

INTRODUCTION

Brillouin microlasers were first studied about a decade ago [1–4], and have emerged as a powerful platform for narrow linewidth operation. Unlike conventional lasers, Brillouin devices derive optical gain through a process that is parametric in nature, but that resembles stimulated emission on account of damping of the phonons involved in the amplification process [5]. The phonon participation drastically impacts the fundamental linewidth of the Brillouin laser, increasing it by about 600 fold (equal to the number of thermal Brillouin quanta at the operating temperature) relative to the quantum limit [6], and leading to a temperature dependent linewidth [7]. Otherwise, the linewidth formula is Schawlow-Townes like in the way that it scales inversely with optical power and roughly inverse-quadratically with cavity Q factor [8]. These features provide a way to reduce fundamental linewidth even in the presence of the large thermal noise contribution. The parametric nature of the Brillouin process also allows pump frequency noise to leak into the laser frequency noise [9]. However, this leakage is strongly suppressed when the optical cavity damping is low relative to the phonon damping.

Nonetheless, as chip-based devices Brillouin lasers present considerable challenges for narrow linewidth operation. For example, specialized processing methods are required to attain the highest possible optical Q factors. Also, thermo-refractive noise [10, 11], which scales about inversely with mode volume, is a significant source of noise, especially at low offset frequencies. Even with these challenges, early work attained Brillouin fundamental linewidths below 1 Hz [6]. Frequency stability improvement was also demonstrated by locking these devices to compact reference cavities [12]. Also significant, the application of chip-based Brillouin devices to microwave synthesis [13, 14] and Sagnac gyroscopes [15–17] showed that thermorefractive noise and pump noise do not significantly impact the relative coherence of co-lasing Stokes waves (i.e., their beatnote linewidth). Thus, such specific operational modalities can leverage the narrow fundamental linewidths of chip-based Brillouin lasers. Towards full integration, narrow-linewidth Brillouin laser designs have also emerged that feature integrated waveguides [16, 18, 19]. If combined with pump sources, they could potentially provide robust sources of high coherence light.

Here, we report measurement of an ultra-low frequency noise level of 9 mHz·Hz/Hz in an on-chip stimulated Brillouin laser (SBL) at an output power of 0.9 mW. Both the noise level and its power dependence when compared to theory [6] suggest that it is fundamental in origin and would correspond to a linewidth of 60 mHz. This linewidth is 5× lower than in previous reports, and to measure it an enhancement of the self-heterodyne optical frequency discriminator method [20–22] is applied. Indeed, the current frequency noise measurement provides a way to test and analyze this noise measurement method. The ultra-low noise level is made possible by the high optical Q of the resonator in combination with higher single-mode optical power through suppression of Brillouin cascade [23].

BACKGROUND ON BRILLOUIN CASCADE

Phase matching for efficient Brillouin laser oscillation requires that the frequency separation between the pumped resonator mode and Stokes laser mode equals the Brillouin shift frequency (to within the Brillouin gain bandwidth). For counter-propagating pump and Stokes waves in the silica resonators studied here, the shift is about 10.8 GHz for pumping near 1550 nm. Matching this shift to within the Brillouin gain bandwidth is readily accomplished by microfabrication control of the resonator diameter, which aligns the free-spectral-range (FSR) of the resonator to the Brillouin shift frequency [4]. However, because FSR dispersion is small compared with the gain bandwidth, the neighboring longitudinal mode readily phase matches to the initial Stokes laser wave, and it will lase (i.e., lasing cascade [6]) when the initial Stokes power reaches a certain threshold (Fig. 1a, upper panel). Cascading effectively clamps the laser power of the first Stokes wave (now the pumping wave) and increases its noise due to the second order Stokes wave [23], both of which are undesirable for ultra-low-noise appli-

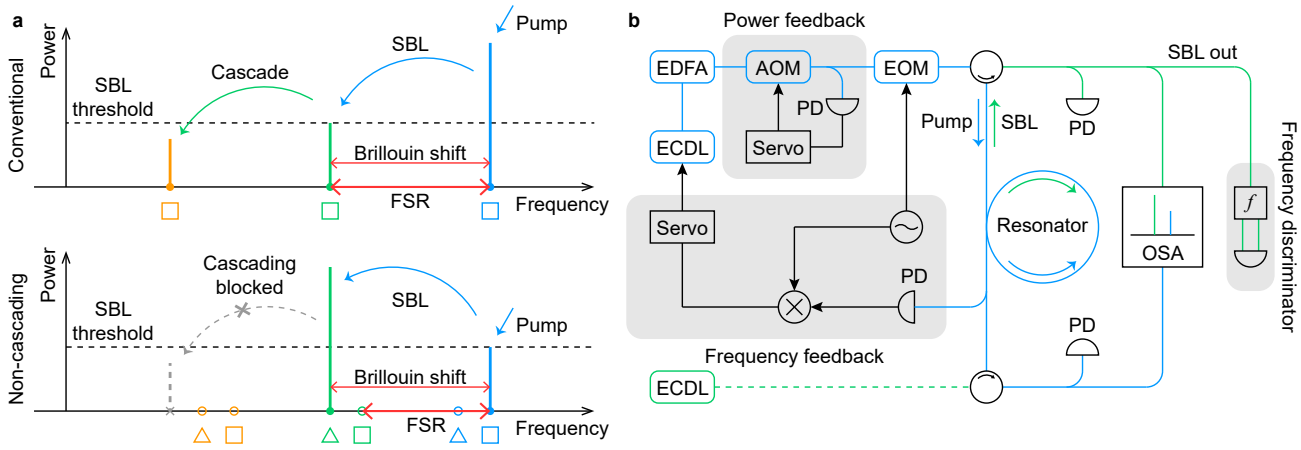

FIG. 1. **Operation of Brillouin lasers and experimental setup. a**. Upper panel: spectral diagram for conventional Brillouin laser operation, where the FSR is matched to the Brillouin frequency shift. Lower panel: spectral diagram for non-cascading laser operation, where FSR is mismatched from the Brillouin shift. Markers below the modes indicate two transverse mode families. Modes with the same marker shape belong to the same mode family. **b**. Experimental setup. An external-cavity diode laser (ECDL) is amplified by an erbium-doped fiber amplifier (EDFA) and sent to a tapered fiber for coupling to the resonator. The laser power is actively stabilized by an acousto-optic modulator (AOM) with power feedback from a photodetector (PD). The laser frequency is Pound-Drever-Hall (PDH) locked to the resonance using an electro-optic modulator (EOM) and the error signal feeds back directly into ECDL. The Brillouin laser wave, propagating in the opposite direction of the pumping, is collected with a circulator. An optical spectrum analyzer (OSA) is used to monitor pump and SBL spectra and to ensure that no cascading occurs. The laser output is also sent to an optical frequency discriminator to measure the frequency noise. An auxiliary ECDL launched in the opposite direction to the pump is used for Q and dispersion measurements. The detailed description of the optical frequency discriminator is provided in Fig. 3a.

cations. The introduction of dispersion within the same mode family during microfabrication [24] or the use different transverse mode families for pumping and Stokes oscillation [1, 2], as employed here, will block the cascading action (see Fig. 1a, lower panel) so that Brillouin laser power can increase well beyond the normal cascade threshold point.

To inhibit cascade in this work, a silica wedge resonator [4] is fabricated with an FSR of 8.9 GHz (smaller than the Brillouin shift of around 10.7 GHz), which thereby prevents cascade within any of the longitudinal mode families. Phase matching is then provided by pumping and laser oscillation on modes belonging to different transverse mode families. Because the resonator features a moderate density of very-high-Q modes within one FSR [25], the mode selection to enable phase matching is relatively straightforward and is described below. The high optical Q factor of both modes is important because the laser threshold power is inversely proportional to both the pump mode Q and the SBL mode Q. The experimental setup is described in Fig. 1b.

PUMP AND SBL MODE SELECTION

To locate phase-matched high-Q mode-pairs in the resonator, the dispersion of several mode families is measured using a tunable external-cavity diode laser (ECDL) together with a calibrated Mach-Zehnder interferometer [26]. Measurements of several transverse mode families (index m) plotted versus longitudinal mode number μ are presented in Fig. 2. Before plotting, a constant offset frequency ν_0 (here taken as the SBL frequency) is subtracted as well as a linear dispersion term equal to $\mu \times \mathrm{FSR}$ where FSR is the free spectral range of the Brillouin laser mode (see below). The plotted lines are therefore given by: $\Delta\nu_\mu^m \equiv \nu_\mu^m - \nu_0 - \mu \times \mathrm{FSR}$, where ν_μ^m is the frequency of longitudinal mode μ belonging to transverse mode family m.

Two mode families are highlighted using blue and green data points. Simulated mode field distributions of these two modes are shown in the Fig. 2 inset, and the modes are determined to be the TM2 (green) and TM4 (blue). The TM2 mode is selected as the lasing mode and the plot uses its FSR in the calculation of $\Delta\nu_\mu^m$. As a result, the green data points appear horizontal in the plot. Both of these mode families feature high intrinsic Q-factors around 400 million and also experience only a few mode crossings over a wide wavelength band. The pump mode must be located one Brillouin shift higher in frequency relative to the laser mode frequency. This condition, represented by the red phase-matching line in Fig. 2, is wrapped (modulo the Brillouin shift) in making the plot, and the pumping wavelength is determined

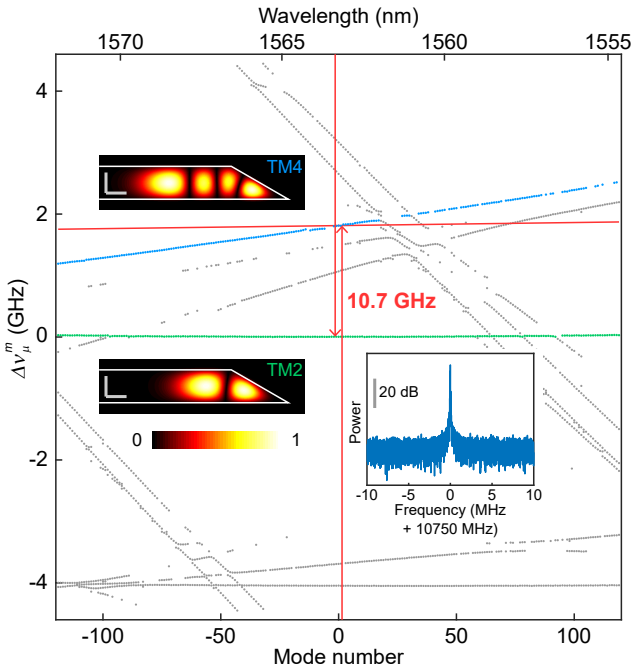

FIG. 2. **Mode selection for non-cascading Brillouin laser operation.** Mode dispersion of the resonator is measured over a spectral region spanning several hundred longitudinal mode numbers. The intended SBL mode family (TM2) is highlighted in green and its corresponding pump phase-matching line is shown in red. The intended pump mode family (TM4) is highlighted in blue. First order dispersion is introduced into the plot so that the laser mode family data points appear horizontal. **Left insets**. Simulated electric field distributions (norm) of the TM4 and TM2 modes. Scale bars are 5 μm. **Lower right inset**. Measured electrical spectrum of the pump and Brillouin laser beatnote signal.

to be around 1563 nm. The lasing threshold is 0.9 mW and the generated laser output power exceeds 0.9 mW at pumping power of 35.7 mW. The beatnote of pump and SBL signals is also shown as an inset in Fig. 2.

CROSS-CORRELATION METHOD

The self-heterodyne optical frequency discriminator approach [20–22] was first applied to measure the frequency noise spectral density of the generated laser signal (Fig. 3a). However, at high offset frequencies (above 1 MHz), the frequency noise floor and measurement sensitivity were found to be limited by technical noise from the photodetector (PD), which is quantified by the noise equivalent power (NEP). This technical noise prevented measurement of fundamental frequency noise below $0.1\text{Hz}^2/\text{Hz}$. To overcome this limitation, we applied cross correlation (XCOR) of the electrical signals produced at the interferometer output. Electrical oscillators employ XCOR with a reference oscillator to measure phase noise [27] and it has also been applied recently to measure frequency-comb generated microwave signals by heterodyne with two reference comb signals [28]. The present measurement is distinct in applying XCOR to optical phase noise measurement, and also does not require reference optical or radio frequency oscillators. Moreover, the very low frequency noise of the device studied here illustrates the power of XCOR to boost sensitivity in this context.

As shown in Fig. 3a, the measurement setup employs an AOM to split the input light into frequency-shifted (1^{st} order output) and un-shifted parts (0^{th} order output), the latter being delayed by a 1-km-long fiber. However, instead of a single photodetector, two photodetectors receive the optical signals. Their outputs are recorded using an oscilloscope for subsequent XCOR to remove detector technical noise. The AOM is driven with a 55 MHz radio-frequency signal, which also determines the carrier frequency of the electrical signals from the two PDs. These signals are acquired with an oscilloscope having a 500 MHz sampling rate to prevent aliasing of the signal. AC coupling is used to block the low-frequency components at the oscilloscope. Delays between the channels are estimated to be less than 0.5 ns and are not considered in subsequent analyses. 0.2 seconds of waveform (100×10^6 points in each channel, 200×10^6 points total) are collected and transferred to a computer for processing. Phase signals are extracted with a Hilbert transform. The Hilbert transform creates distortions at the endpoints of the signal, thus the first and last 10 ms (5×10^6 points) for each channel are discarded after the transform. The remaining points are separated into segments (rectangular windowing), each with a 0.1 ms length (corresponding to a resolution bandwidth of 10 kHz) and Fourier transformed to extract the phase noise amplitude at a given offset frequency. For offset frequencies less than 200 kHz, resolution bandwidths are made smaller, and the segment lengths are adjusted accordingly. The correlation can then be found as the product between the Fourier coefficients of the two phase signals, averaged over different segments.

The correlation of the frequency noise measured by the cross-correlator contains contributions from both frequency noise and intensity noise:

$$C_\nu(f) = f^2 C_\phi(f) - f^2[C_a(f_c + f) + C_a(f_c - f)] \quad (1)$$

where $C_\phi(f)$ and $C_a(f)$ are the transferred phase and amplitude noise at offset frequency f:

$$C_\phi(f) = [2 - 2\,(1 - \tau_0 \text{BW})^+ \cos(2\pi f \tau)] \frac{1}{f^2} S_\nu(f) \quad (2)$$

$$C_a(f) = [2 + 2\,(1 - \tau_0 \text{BW})^+ \cos(2\pi f \tau)] \frac{1}{4} S_I(f) \quad (3)$$

Here $S_\nu(f)$ and $S_I(f)$ are the two-sided spectral densities of frequency noise and relative intensity noise (RIN) of

the laser, BW is the resolution bandwidth of the cross-correlator (taken as 10 kHz), τ_0 is the delay time of the frequency discriminator measurement setup, and $x^+ = \max(0, x)$ is the ramp function. We assumed that noise at different offset frequencies are independent. The ramp filter term before the $\cos(2\pi f\tau)$ term is an artifact of the rectangular window chosen. Using a window with higher dynamic range decreases the filtering effect at the expense of offset frequency resolution. To separate the frequency noise and RIN, we tune the carrier frequency f_c to an integer multiple of $1/\tau_0$. In this case the correlation reads

$$\begin{aligned} C_\nu(f) = 2\left[1-(1-\tau_0\mathrm{BW})^+\cos(2\pi f\tau_0)\right]S_\nu(f) \\ -\frac{1}{2}\left[1+(1-\tau_0\mathrm{BW})^+\cos(2\pi f\tau_0)\right] \\ \times f^2(S_I(f_c+f)+S_I(f_c-f)) \end{aligned} \tag{4}$$

where the modulations on frequency noise and RIN are now completely out of phase. The DC and $1/\tau_0$ frequency components of the correlations are extracted by filtering and then recombined to remove the intensity noise and estimate the frequency noise. Error bars of each correlation are determined by the variance of the correlation over different signal segments, and then propagated to the estimated frequency noise.

FREQUENCY NOISE MEASUREMENT

A comparison of the measurements both with and without application of the XCOR method is presented in Fig. 3b. Here, the red trace is a phase noise analyzer measurement of the electrical signal produced by detection of a single output from the interferometer, while the blue trace results by applying the XCOR meausurement. Both traces overlap well at low offset frequencies (below 500 kHz), and a single PD is sufficient to measure the frequency noise accurately. At these frequencies noise is believed to be thermo-refractive in origin based on simulations [30] shown in the figure (dashed line). However, at higher offset frequencies, the noise measurement sensitivity is enhanced by 10 to 15 dB using the XCOR method. Here, the detector noise is suppressed by cross correlation. As an aside, the Pound Drever Hall locking loop (see experimental setup in Fig. 1b) has a bandwidth of 10 kHz and we believe it does not influence the measured noise at high offset frequencies.

The rising noise levels at the highest offset frequencies in the XCOR data are not believed to be fundamental and, instead, are attributed to the short averaging time resulting from the limited memory of the oscilloscope. Also, the noise spectra measured using the conventional (non XCOR) approach contain spurs that originate from destructive interference produced by the delay in the interferometer (first order corresponds to $1/\tau_0 = 214$ kHz, where $\tau_0 = 4.67$ ms is the delay time). The spectral modulations resulting from the interference are shown in Fig. 3c, which gives the electrical spectrum of a detected output from the interferometer. These modulations, once digitally removed in the phase noise spectra, leave the spurs as an artifact.

A narrow portion of the measured XCOR spectrum Fig. 3b is approximately white noise like. By averaging the measured frequency noise between 1.5 MHz to 2 MHz, this frequency noise level is estimated to be 9 mHz $\cdot$ Hz/Hz (equivalent to a Lorentzian linewidth of 60 mHz). To investigate the possible origin of this noise we measured the frequency noise noise at several laser power levels. The results are summarized in Fig. 3d and vary inversely with laser power which is consistent with fundamental laser frequency noise. As an additional check, the theoretical fundamental frequency noise level can be calculated and compared to the measured noise. The lasing TM2 mode has a loaded (external) quality factor of $Q_\mathrm{T} = 269\times10^6$ ($Q_\mathrm{ex} = 729\times10^6$). Using the fundamental linewidth formula for the Brillouin laser [6], the two-sided frequency noise of the laser is given by,

$$S_{\nu,\mathrm{F}} = \frac{h\nu_0^3 n_\mathrm{th}}{2Q_\mathrm{T}Q_\mathrm{ex}P_\mathrm{SBL}} \tag{5}$$

where h is the Planck constant, P_SBL is the SBL output power, $\nu_0 = 191.8$ THz is the optical frequency of the SBL and n_th is the thermal occupation of the phonon mode. At room temperature, $n_\mathrm{th} \approx 568$, which gives $S_{\nu,\mathrm{F}} \times P_\mathrm{SBL} = 6.77$ mW $\cdot$ mHz $\cdot$ Hz/Hz. The fundamental frequency noise is plotted in Fig. 3d assuming a zero alpha parameter [29] and is in good agreement with measured data.

It is important to also consider the level of pump frequency noise that couples into the SBL frequency noise, given by

$$S_{\nu,\mathrm{P}} = \left(\frac{\kappa}{\kappa+\Gamma}\right)^2 S_\mathrm{P} \tag{6}$$

where S_P is the two-sided frequency noise of the pump laser, and the factor involving $\kappa = 2\pi\nu_0/Q_\mathrm{T}$ and Γ (the Brillouin gain linewidth) gives the suppression of pump frequency noise by the Brillouin process [9]. The frequency noise of the pump laser (Newport, TLB-6728) was measured to be 90 Hz^2/Hz at 1 MHz offset frequency. This requires a Brillouin suppression factor of about 45 dB in order for coupled pump frequency noise to be less than the measured frequency noise level. Using the measured Q_T in the suppression formula gives a Brillouin gain linewidth of about $\Gamma/(2\pi) = 130$ MHz which is around 3$\times$ larger than in our previous measurements of SBL in silica [6]. This discrepancy might originate from higher-order acoustic mode participation in the two transverse mode SBL generation. Such a mode could have a larger phonon decay rate. Phonon decay

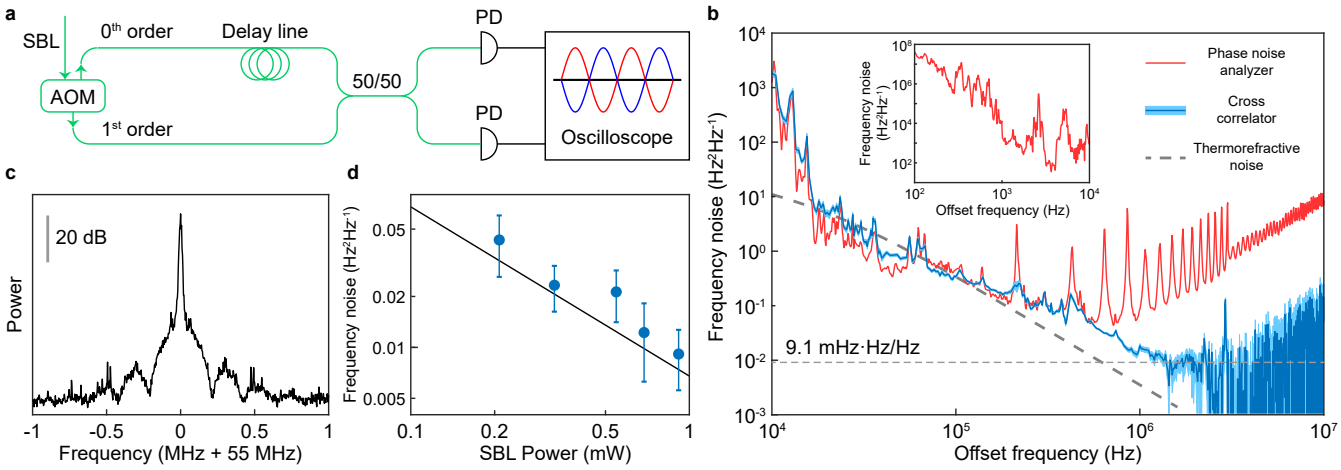

FIG. 3. **Brillouin laser frequency noise measurement. a**. Experimental setup of the optical frequency discriminator in Fig. 1b. **b**. SBL frequency noise measured by conventional optical discriminator method in combination with an electrical phase noise analyzer (red) and by the cross-correlation technique (blue). The light blue shading shows the error range (standard error of the mean). The average frequency noise between 1.5 MHz and 2 MHz offset frequency is 9 mHz · Hz/Hz and is shown as a horizontal dashed line. The dashed curve (dark gray) shows the simulated thermorefractive noise for the laser mode. Inset: low-offset-frequency portion of the frequency noise as measured by the phase noise analyzer. **c**. Electrical spectrum of the frequency discriminator output from a single PD. **d**. Theoretical fundamental frequency noise plotted versus laser output power (black line) [6] assuming a zero alpha parameter [29]. Dots are inferred from measurement data and error bars are standard deviations.

rates as large as 150 MHz have been reported for silica-based structures in the literature [16]. Importantly, the SBL pumping power was varied by attenuation using the AOM (Fig. 1b) so that pump frequency noise S_P did not change during the collection of the data in Fig. 3d. It cannot therefore explain the inverse power dependence observed in Fig. 3d. Nonetheless, the limited spectral span of the white noise data, makes it difficult to completely confirm the origin of the noise. We are currently working towards increasing the spectral span over which ultra-low white noise level is observable.

DISCUSSION

We have demonstrated sub-10 mHz · Hz/Hz fundamental frequency noise levels using a chip-based Brillouin laser. The low noise level results from a combination of the high-Q resonator with increased operational power through non-cascading operation. The frequency noise level was too low to measure using conventional optical discrimination methods and cross-correlation was applied to this technique to obtain a sensitivity boost as large as 15 dB.

Several other strategies might be employed to achieve further noise level improvements. For example, increasing laser power ultimately leads to under-coupling of the pump mode to the resonator caused by back action from the lasing mode. This, in turn, decreases differential efficiency and laser power. To isolate this loading back action, a single-cascading scheme can be used (Fig. 4a), which would block the cascade at the second order (instead of first order). In this configuration, pump loading would remain constant. A calculation showing the potential improvement is provided in Fig. 4b, and a demonstration of this scheme using the same resonator as in the text is shown in Fig. 4c. At yet higher laser powers, parametric oscillation due to the Kerr effect within the transverse mode families could limit operation. However, it should be possible to inhibit this oscillation through dispersion engineering [31] or possible operation in the normal dispersion regime. Finally, operation with reduced amplitude-phase coupling is also important for minimization of the Brillouin laser linewidth [29].

Overall, the results presented here demonstrate the potential for silica-based high-Q laser platforms to achieve extremely narrow fundamental laser linewidths. Even while the noise at low offset frequencies remains high, these noise sources can be suppressed in applications such as the Sagnac gyroscope that rely upon relative noise of co-lasing waves. Likewise, applications that are sensitive to only short-term frequency noise can benefit from these improvements.

Data availability. The data that support the plots within this paper and other findings of this study are available from the corresponding author upon reasonable request.

Funding. Air Force Office of Scientific Research (FA9550-18-1-0353) and the Caltech Kavli Nanoscience

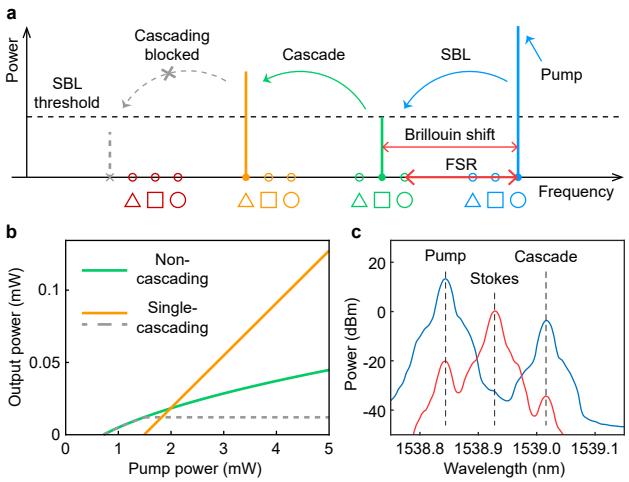

FIG. 4. **Proposed single-cascading Brillouin laser pumping scheme. a**. Spectral diagram for single-cascading Brillouin laser operation. Markers below the modes indicate their transverse mode families. **b**. Calculated output laser power versus pump power for non-cascading (green) and single-cascading (orange) pumping schemes, assuming constant external coupling to resonator modes from the tapered fiber. Dashed gray line shows the output power of the first Stokes mode in the single-cascading pumping scheme, which is clamped at the lasing threshold when the first-order cascaded mode start to lase. **c**. Measured optical spectrum traces showing single-cascading SBL action. Blue and red traces are the forward and backward output power from the resonator, showing the pump, Stokes and cascade modes, and second-order cascade lasing is not observed.

Institute.

Acknowledgment. The authors acknowledge Q. Yang and Y. Lai for helpful discussions.

Disclosures. The authors declare no conflicts of interest.

[1] I. S. Grudinin, A. B. Matsko, and L. Maleki, Phys. Rev. Lett. **102**, 043902 (2009).
[2] M. Tomes and T. Carmon, Phys. Rev. Lett. **102**, 113601 (2009).
[3] R. Pant, C. G. Poulton, D.-Y. Choi, H. Mcfarlane, S. Hile, E. Li, L. Thevenaz, B. Luther-Davies, S. J. Madden, and B. J. Eggleton, Opt. Express **19**, 8285 (2011).
[4] H. Lee, T. Chen, J. Li, K. Y. Yang, S. Jeon, O. Painter, and K. J. Vahala, Nat. Photon. **6**, 369 (2012).
[5] Y. R. Shen and N. Bloembergen, Phys. Rev. **137**, A1787 (1965).
[6] J. Li, H. Lee, T. Chen, and K. J. Vahala, Opt. Express **20**, 20170 (2012).
[7] M.-G. Suh, Q.-F. Yang, and K. J. Vahala, Phys. Rev. Lett. **119**, 143901 (2017).
[8] A. L. Schawlow and C. H. Townes, Phys. Rev. **112**, 1940 (1958).
[9] A. Debut, S. Randoux, and J. Zemmouri, Phys. Rev. A **62**, 023803 (2000).
[10] M. L. Gorodetsky and I. S. Grudinin, J. Opt. Soc. Am. B **21**, 697 (2004).
[11] A. B. Matsko, A. A. Savchenkov, N. Yu, and L. Maleki, J. Opt. Soc. Am. B **24**, 1324 (2007).
[12] W. Loh, A. A. Green, F. N. Baynes, D. C. Cole, F. J. Quinlan, H. Lee, K. J. Vahala, S. B. Papp, and S. A. Diddams, Optica **2**, 225 (2015).
[13] J. Li, H. Lee, and K. J. Vahala, Nat. Commun. **4**, 2097 (2013).
[14] J. Li, X. Yi, H. Lee, S. A. Diddams, and K. J. Vahala, Science **345**, 309 (2014).
[15] J. Li, M.-G. Suh, and K. Vahala, Optica **4**, 346 (2017).
[16] S. Gundavarapu, G. M. Brodnik, M. Puckett, T. Huffman, D. Bose, R. Behunin, J. Wu, T. Qiu, C. Pinho, N. Chauhan, *et al.*, Nat. Photon. **13**, 60 (2019).
[17] Y.-H. Lai, M.-G. Suh, Y.-K. Lu, B. Shen, Q.-F. Yang, H. Wang, J. Li, S. H. Lee, K. Y. Yang, and K. Vahala, Nat. Photon. **14**, 345 (2020).
[18] N. T. Otterstrom, R. O. Behunin, E. A. Kittlaus, Z. Wang, and P. T. Rakich, Science **360**, 1113 (2018).
[19] K. Y. Yang, D. Y. Oh, S. H. Lee, Q.-F. Yang, X. Yi, B. Shen, H. Wang, and K. Vahala, Nat. Photon. **12**, 297 (2018).
[20] M. Van Exter, S. Kuppens, and J. Woerdman, IEEE J. Quantum Electron. **28**, 580 (1992).
[21] H. Ludvigsen, M. Tossavainen, and M. Kaivola, Opt. Commun. **155**, 180 (1998).
[22] W. Jin, Q.-F. Yang, L. Chang, B. Shen, H. Wang, M. A. Leal, L. Wu, A. Feshali, M. Paniccia, K. J. Vahala, and J. E. Bowers, arXiv:2009.07390 (2020).
[23] R. O. Behunin, N. T. Otterstrom, P. T. Rakich, S. Gundavarapu, and D. J. Blumenthal, Phys. Rev. A **98**, 023832 (2018).
[24] M. Puckett, D. Bose, K. Nelson, and D. J. Blumenthal, in *CLEO: Science and Innovations* (Optical Society of America, 2019) pp. SM4O–1.
[25] L. Wu, H. Wang, Q.-F. Yang, Q.-X. Ji, B. Shen, C. Bao, M. Gao, and K. Vahala, Opt. Lett. **45**, 5129 (2020).
[26] X. Yi, Q.-F. Yang, K. Y. Yang, M.-G. Suh, and K. Vahala, Optica **2**, 1078 (2015).
[27] W. F. Walls, in *Proceedings of the 1992 IEEE Frequency Control Symposium* (IEEE, 1992) pp. 257–261.
[28] X. Xie, R. Bouchand, D. Nicolodi, M. Giunta, W. Hänsel, M. Lezius, A. Joshi, S. Datta, C. Alexandre, M. Lours, *et al.*, Nat. Photon. **11**, 44 (2017).
[29] Z. Yuan, H. Wang, L. Wu, M. Gao, and K. Vahala, Optica **7**, 1150 (2020).
[30] N. Kondratiev and M. Gorodetsky, Phys. Lett. A **382**, 2265 (2018).
[31] K. Y. Yang, K. Beha, D. C. Cole, X. Yi, P. Del'Haye, H. Lee, J. Li, D. Y. Oh, S. A. Diddams, S. B. Papp, *et al.*, Nat. Photon. **10**, 316 (2016).